

Comparison between non orographic gravity wave parameterizations used in QBOi models and Strateole 2 constant level balloons

F. Lott¹, R. Rani¹, C. McLandress⁴, A. Podglagen¹, A. Bushell⁵, M. Bramberger⁹, H.-K. Lee⁶, J. Alexander⁹, J. Anstey⁴, H.-Y. Chun⁶, A. Hertzog², N. Butchart⁵, Y.-H. Kim⁷, Y. Kawatani¹⁷, B. Legras¹, E. Manzini⁸, H. Naoe¹⁰, S. Osprey¹¹, R. Plougonven³, H. Pohlmann⁸, J. H. Richter¹², J. Scinocca⁴, J. García-Serrano¹³, F. Serva¹⁴, T. Stockdale¹⁵, S. Versick¹⁶, S. Watanabe¹⁷, K. Yoshida¹⁷

¹Laboratoire de Météorologie Dynamique (LMD)/IPSL, PSL Research Institute, Ecole Normale

Supérieure, Paris, France.

²LMD/IPSL, Sorbone Université, Paris, France.

³LMD/IPSL, Ecole Polytechnique, Institut Polytechnique de Paris, Palaiseau, France

⁴Canadian Centre for Climate Modelling and Analysis (CCCma), Victoria, Canada

⁵Met Office, FitzRoy Road, Exeter, UK

⁶Yonsei University, Seoul, South Korea

⁷Institut für Atmosphäre und Umwelt, Goethe-Universität, Frankfurt am Main, Germany

⁸Max Planck Institute for Meteorology, Hamburg, Germany

⁹NorthWest Research Associates, Boulder Office, Boulder, CO, USA

¹⁰Meteorological Research Institute (MRI), Tsukuba, Japan

¹¹Atmospheric, Oceanic and Planetary Physics, University of Oxford, Oxford, UK

¹²National Center for Atmospheric Research (NCAR), Boulder, Colorado, USA

¹³Group of Meteorology Universitat de Barcelona, Barcelona, Spain

¹⁴Institute of Marine Sciences, National Research Council, Rome, Italy

¹⁵European Centre for Medium-Range Weather Forecasts (ECMWF), Reading, UK

¹⁶Karlsruher Institut für Technologie (KIT), Karlsruhe, Germany

¹⁷Japan Agency for Marine-Earth Science and Technology (JAMSTEC), Yokohama, Japa

Key Points:

- The 3 standard non-orographic gravity waves (GWs) parameterizations tuned to produce a realistic tropical quasi-biennial oscillation in 12 global climate models are used to predict in-situ balloon observations.
- Parameterized GWs needed in large-scale models have realistic amplitudes in the tropical lower stratosphere.
- Balloon averaged and daily values of GWs momentum fluxes can correlate with observations when the parameterized GWs are coming from the lower and middle troposphere.
- The probability density distributions can also be realistically reproduced, but problem arises for parameterizations that try to relate gravity waves to their convective sources.

Version 6, date: February 7, 2024

Corresponding author: Francois Lott, flott@lmd.ens.fr

Abstract

Gravity Waves (GWs) parameterizations from 12 General Circulation Models (GCMs) participating to the Quasi-Biennial Oscillation initiative (QBOi) are directly compared to Strateole-2 balloon observations made in the lower tropical stratosphere from November 2019 to February 2020 (phase 1) and from October 2021 and January 2022 (phase 2). The parameterizations used span the 3 standard techniques used in GCMs to represent subgrid scale non-orographic GWs, namely the two globally spectral techniques developed by Warner and McIntyre (1999) and Hines (1997) respectively and the "multiwaves" approaches following Lindzen (1981). The input meteorological fields necessary to run the parameterizations offline are extracted from the ERA5 reanalysis and correspond to the instantaneous meteorological conditions found underneath the balloons. In general, the amplitudes are in fair agreement between measurements of the momentum fluxes due to waves with periods less than 1 hr and the parameterizations. The correlation between the daily observations and the corresponding results of the parameterization can be around 0.4, which is 99% significant since 1200 days of observations are used. Given that the parameterizations have only been tuned to produce a QBO in the models, the 0.4 correlation coefficient of the GW parameters is surprisingly good. These correlations nevertheless vary considerably between schemes and depend little on their formulation (globally spectral versus multiwaves for instance). We therefore attribute it to dynamical filtering all schemes taking good care of it, whereas only few relate the gravity waves to their sources. Except for two parameterizations, significant correlations are mostly found for eastward propagating waves, which may be due to the fact that during both Strateole 2 phases the QBO is easterly at the altitude of the balloon flights. We also found that the pdfs of the momentum fluxes are better represented in spectral schemes with constant sources than in schemes ("spectral" or "multiwaves") that relate GWs to their convective sources.

Plain Language Summary

In most large-scale atmospheric models, gravity wave parameterizations are based on well understood but simplified theories and parameters which are keyed to reduce systematic errors on the planetary scale winds. In the equatorial regions, the most challenging errors concern the Quasi Biennial Oscillation. Although it has never been verified directly, it is expected that the parameterizations tuned this way should transport a realistic amount of momentum flux in both the eastward and westward directions when compared to direct observations. Here we show that it is the case, to a certain extent, using constant-level balloon observations at 20 km altitude. The method consists in comparing directly, each day and at the location of the balloon the measured momentum fluxes and the estimations from the gravity wave parameterizations used in the global models that participate to the Quasi-Biennial Oscillation initiative and when using observed values of the large-scale meteorological conditions of wind, temperature, precipitation, and diabatic heating.

81 **1 Introduction**

82 It is well known that the large scale circulation in the middle atmosphere is in good
 83 part driven by gravity waves (GWs) that propagate in the stratosphere and mesosphere
 84 (Andrews et al., 1987). These waves carry horizontal momentum vertically and inter-
 85 act with the large scale flow when they break. Since the horizontal scale of these waves
 86 can be quite short, much shorter than the horizontal scale of conventional atmospheric
 87 General Circulation Models (GCMs) they need to be parameterized (Alexander & Dunker-
 88 ton, 1999). In the tropics, the convective GWs are believed to largely dominate (Fovell
 89 et al., 1992; Alexander et al., 2000; Lane & Moncrieff, 2008), they contribute significantly
 90 to the forcing of the Quasi-Biennial Oscillation (QBO), a near 28-month oscillation of
 91 the zonal mean zonal winds that occurs in the lower part of the equatorial stratosphere
 92 (Baldwin et al., 2001). For these reasons, convectively generated GWs must be param-
 93 eterized in order to simulate a QBO in most GCMs.

94 Although gravity wave parameterizations are now used in many models with suc-
 95 cess including in the tropics (Scinocca, 2003; Song & Chun, 2005; Beres et al., 2005; Orr
 96 et al., 2010; Lott & Guez, 2013; Bushell et al., 2015; Anstey et al., 2016; Christiansen
 97 et al., 2016; Serva et al., 2018), their validation using direct in situ observations remains
 98 a challenge. Large horizontal-scale GWs can be obtained from global satellite observa-
 99 tions of temperature (Geller et al., 2013) and the corresponding momentum flux com-
 100 puted using polarization relations (Alexander et al., 2010; Ern et al., 2014). In order to
 101 observe the shorter horizontal scales that force the QBO and to have a direct measure-
 102 ment of the corresponding momentum flux, in situ observations are essential. The most
 103 precise ones are provided by constant-level long-duration balloons, like those made in
 104 the Antarctic region during Strateole-Vorcore (Hertzog, 2007) and Concordiasi (Rabier
 105 et al., 2010), or in the deep tropics during PreConcordiasi (Jewtoukoff et al., 2013) and
 106 Strateole 2 (Haase et al., 2018). Among many important results, these balloon obser-
 107 vations have shown that the momentum flux entering in the stratosphere is extremely
 108 intermittent (Hertzog et al., 2012). This intermittency implies that the mean momen-
 109 tum flux is mostly transported by few large-amplitude waves that potentially break at
 110 lower altitudes than when the GW field is more temporally uniform. This intermittent
 111 character, when reproduced by a parameterization (de la Cámara et al., 2014; Kang et
 112 al., 2017; Alexander et al., 2021), can help reduce systematic errors in the midlatitudes,
 113 such as the timing of the final warming in the Southern Hemisphere polar stratosphere
 114 (de la Cámara et al., 2016), or on the simulation of the QBO (Lott et al., 2012). Bal-
 115 loon observations have also been used to characterize the dynamical filtering by the large
 116 scale winds (Plougonven et al., 2017), and to validate the average statistical properties
 117 of the GW momentum flux predicted offline using reanalysis data (Kang et al., 2017; Alexan-
 118 der et al., 2021).

119 However, the evaluations of parameterizations using balloon observations done in
 120 the past were often quite indirect, and concerned more their statistical behaviours (Jewtoukoff
 121 et al., 2015; Kang et al., 2017; Alexander et al., 2021) rather than their ability to directly
 122 predict instantaneous values of momentum fluxes. Maybe a good reason to consider global
 123 statistical properties rather than daily predictions is that parameterizations are based
 124 on simplified quasi-linear wave theory, assume spectral distributions that are loosely con-
 125 strained, and ignore lateral propagation almost entirely (some attempt to include it can
 126 be found in Amemiya and Sato (2016), see also the underlying theory in Achatz et al.
 127 (2023)). Nevertheless, some factors could mitigate these weaknesses. One is that in most
 128 parameterizations the wave amplitude is systematically limited by a breaking criterion
 129 that encapsulates nonlinear effects. Another is that some parameterizations explicitly
 130 relate launched waves to sources, and there is constant effort to improve the realism of
 131 the convective ones (Liu et al., 2022). Also, observations systematically suggest that dy-
 132 namical filtering by the large scale wind is extremely strong for upward propagating GWs
 133 (Plougonven et al., 2017), and this central property is represented in most GW param-

134 eterizations. For all these reasons, it may well be that GW parameterizations using the
135 large scale flow found at a given place and time gives MFs that can be directly compared
136 to the MFs measured by a balloon at the same place.

137 Based on the relative success of the offline calculations done in the past using re-
138 analysis data (Jewtoukoff et al., 2015; Kang et al., 2017; Alexander et al., 2021), Lott
139 et al. (2023) have shown that such a direct comparison gives result of interest. The first
140 is that the state of the art convective gravity wave drag scheme of Lott and Guez (2013)
141 predicts momentum fluxes in the low equatorial stratosphere whose amplitudes can be
142 directly compared with those measured during phase 1 of the Strateole-2 balloon cam-
143 paign. This gives a direct in-situ observational confirmation that the theories and mod-
144 elling of the QBOs developed over the last 50 years are largely correct about the impor-
145 tance of the GWs to the QBO forcing. Moreover, the comparison showed a good level
146 of correlation between the day to day variability in momentum fluxes between measured
147 and parameterized fluxes, a correlation that is much better for waves carrying momen-
148 tum fluxes in the eastward direction than in the westward direction. It was suggested
149 that such a good correlation was due to the fact that the Lott and Guez (2013)'s scheme
150 analysed relate the gravity waves to their convective sources (not all schemes do) and
151 that the GWs experience significant dynamical filtering in the middle troposphere and
152 lower stratosphere. However, Lott et al. (2023) also show that a scheme that relates grav-
153 ity waves to convection only failed to predict the right statistical behaviour of the mo-
154 mentum fluxes, with the probability density function of the momentum flux amplitudes
155 showing long tails for low values of the MFs. This suggests that the parameterization
156 misses processes like lateral propagation or the presence of a background of waves whose
157 origin remains a challenge to predict.

158 The purpose of this paper is to continue the direct comparison used in Lott et al.
159 (2023) by including more recent Strateole 2 observations and nearly all the gravity wave
160 parameterization schemes used by the modelling groups participating to the Quasi-Biennial
161 Oscillation initiative (QBOi, Butchart et al., 2018). We will follow Lott et al. (2023) and
162 use the 8 balloons of the first phase of the Strateole 2 campaign that flew in the lower
163 tropical stratosphere between November 2019 and February 2020 and add the 15 bal-
164 loons that flew more than one day during the second phase of the Strateole 2 campaign,
165 between October 2021 and January 2022. In those flights and each time, we have iden-
166 tified the grid point in the ERA5 reanalysis (Hersbach et al., 2020) that is nearest to the
167 balloon observation and used the vertical profiles of wind and temperature as well as the
168 surface value of precipitations to emulate the parameterization of GWs used in the global
169 models that participated to QBOi. We also extract from the analysis and the associated
170 3hr forecast the analysis uses, the diabatic heatings and the cloud base and top altitudes
171 needed in some schemes to predict gravity waves.

172 The plan of the paper is as follows. Section 2 describe the data and the parame-
173 terization schemes used, section 3 discusses the results in terms of daily correlations, as
174 well as global average and statistics. Section 4 summarizes the results. As we shall see
175 the performances of each parameterization can be contrasted regarding that we use one
176 criteria rather than other, but our purpose is not to promote one scheme in front of the
177 others. Adapting other groups parameterization to a testbed that have been intensively
178 used for one particular parameterization in the past can give an unfair advantage to the
179 later, which is absolutely not the objective of the present work. We return to this point
180 in Section 4.

2 Data and method

2.1 Parameterizations of non orographic gravity wave schemes

The parameterization schemes used to predict non-orographic gravity waves belongs to two well separated families, dating back from the 1980's when it becomes evident that a good simulation of the middle atmosphere by global atmospheric models could not be done without including subgrid scale GWs. The first family roots in the formulation by Lindzen (1981), where the gravity wave field is represented by gravity waves that are monochromatic in the horizontal and time. It was extended to treat a large ensemble of waves by Alexander and Dunkerton (1999) making the assumption that the breaking of each wave could be made independent from the others. An advantage of such schemes is that it roots in linear theories where sources like convection and/or fronts can be introduced using closed form theories (Beres et al., 2005; Song & Chun, 2005; Richter et al., 2010a; Lott & Guez, 2013; de la Cámara & Lott, 2015). In the following we will refer to such schemes as "multiwave", they are expensive because they request a large amount of harmonics to represent well a realistic wave field, but this limit can easily be circumvented by using stochastic approaches (Eckermann, 2011; Lott et al., 2012). As an alternative, but also to better represent breaking, globally spectral schemes have been developed and tested with success. These schemes use the observational fact that GWs produce kinetic energy spectra which have a quite universal shape when expressed as a function of vertical wavenumber. In the early 1990's Hines (1991) developed a theory where GW breaking is represented by imposing an upper limit to the range of vertical wavenumber, the limit being calculated according to the large scale wind and including a Doppler spreading by the other gravity waves (see also Hines, 1997). The scheme has been implemented with success in various GCMs (see for instance Manzini, McFarlane, & McLandress, 1997), and will be referred to as "HDS" for "Hines Doppler Spread" in the following. As an alternative, the theory in Warner and McIntyre (1996) imposes gravity wave saturation according to an empirical spectra but treat vertical changes in the spectra following GWs propagation invariant character. The theory has been simplified and/or optimized to permit implementation, for instance in the UKMO model (Warner & McIntyre, 1999; Scaife et al., 2002) and in the CMAM model (Scinocca, 2003) respectively, and will be referred to as "WMI" for "Warner and McIntyre" in the following. To a certain extent, the spectral schemes can also take into account the relation with sources, for instance the HDS scheme has been related to fronts in Charron and Manzini (2002), and the UKMO version of the WMI scheme to precipitations in Bushell et al. (2015).

In the present paper, we are going to compare the GWs schemes used in 12 of the models that participate to QBOi, all belonging to one of the three type of schemes described above (WMI, HDS, and Multiwave). As all the multiwave schemes used relate GWs to their convective sources and as only one of the spectral scheme is doing so, the UMGA7gws WMI scheme in Bushell et al. (2015), the former will be discussed with the source-related multiwave schemes.

Among the 12 models, three use the Scinocca (2003)'s version of WMI, CMAM, IFS and ECEarth, their version for QBOi are further detailed in Anstey et al. (2016), Orr et al. (2010), and Davini et al. (2017) respectively. They essentially differ by four parameters, the launch level pressure p_l , the launched momentum flux F_{LT} , the characteristic vertical wavenumber m_* and a minimum intrinsic phase speed in the launched spectra, the values of each being given here in Table 1. Note that for EC-Earth the exact value of the parameters in Table 1 are from J. García-Serrano (private communication).

Still among the 12 models, 5 uses the HDS parameterization presented in Manzini et al. (1997): ECham5, MIROC, MPIM, MRI-ESM, and EMAC, their version for QBOi are described in Serva et al. (2018), Watanabe et al. (2011), Pohlmann et al. (2013), Naoe and Yoshida (2019), and Jöckel et al. (2010) (see also Roeckner et al. (2006)) respectively. Between them change the launching level p_l , the root mean square of the horizontal wind

	p_t	F_{LT}	$2\pi/m_*$	C_{\min}
CMAM	100hPa	1.3mPa	1km	0.25 m/s
IFS	450hPa	5mPa	3km	0.5 m/s
ECEarth	450hPa	3.75mPa	2km	0.25 m/s
UMGA7gws	1000hPa	$\sqrt{\text{Precip}}$	4.3km	not used

Table 1. WMI Parameters changing between CMAM, IFS, ECEarth, and UMGA7gws. UMGA7gws is shown distinctly because it is based on (Warner & McIntyre, 1999) simplified version of WMI rather than on (Scinocca, 2003)’s and realte launched MF to precipitations.

	p_t	σ_s	$2\pi/K^*$	$2\pi/m_{\min}$	C_{smo}	N_{smo}
ECham5	600hPa	$1. \pm 0.2$ m/s	125km	0	2	5
MIROC	650hPa	0.95 m/s	250 km	94 km	2	2
MPIM	650hPa	1.2 m/s	125 km	0	2	2
MRI-ESM	700hPa	1.9 m/s	1250 km	190 km	4	2
EMAC	650hPa	1. m/s	125 km	0	2	2

Table 2. HDS Parameters changing between ECHam5, MIROC, MPIM, MRI-ESM, and EMAC.

	p_t	Phase Speed	Δz	Source
LMDz	500hPa	-30m/s<Intrinsic<30m/s	1km	Precip ²
HadGEM2	850hPa-100hPa	-100m/s<Absolute<100m/s	1km-15km	(Convective Heating) ²
WACCM	1000hPa-100hPa	-100m/s<Absolute<100m/s	1km-4km	(Convective Heating) ²

Table 3. Some parameters changing between LMDz, HadGEM2 and WACCM, for information only the schemes being extremely distinct one from the other

233 variability due to GWs at launch level σ , and the effective horizontal wavenumber K^*
 234 (see Table 2). There are also more numerical parameters that eventually changes, a min-
 235 imum value for the cutoff vertical wavenumber m_{\min} , and two parameters that control
 236 smoothing in the vertical of the GWs root mean square variance and cut-off vertical wavenum-
 237 ber, the coefficient C_{smo} and the number of time the smoothing is applied N_{smo} . Im-
 238 portantly nevertheless, in ECham5 the choice has been made to chose the variability pa-
 239 rameter σ randomly, with a normal distribution centered at 1m/S with standard devi-
 240 ation 0.2m/s. The usefulness of such a stochastic ingredient was initially proposed by
 241 Piani et al. (2004) who found that it can help stabilizing the QBO variability in large
 242 scale models and over decades.

243 Finally the last 4 schemes we consider all links GWs to sources (convection or pre-
 244 cipitation), 3 are multiwaves and have been developed independently one from the oth-
 245 ers: LMDz, HadGEM2, and WACCM, their version for QBOi are described in Lott and
 246 Guez (2013), Song and Chun (2005), and Richter et al. (2010b) and 1 uses the ultra sim-
 247 ple version of the WMI schemes presented in Bushell et al. (2015) rather than the Scinocca
 248 (2003)'s version. Note nevertheless that for both HadGEM2 and WACCM, we do not
 249 use the exact version used in QBOi models but rather offline versions developed by Kang
 250 et al. (2017) and Alexander et al. (2021) respectively, and which were adapted to inter-
 251 pret observations. The differences between the 3 multiwave schemes are numerous it is
 252 impossible to detail them, the reader is referred to the corresponding papers, but some
 253 salient differences are in the source term, the launching levels and the intrinsic phase speed
 254 of the launched waves. More specifically, in LMDz is made the choice to relate the launched
 255 MF to square precipitation P_r^2 consistent with linear theory before breaking (Lott & Guez,
 256 2013) whereas in (Bushell et al., 2015) it is related to $\sqrt{P_r}$ (see Table 1). Still in LMDz,
 257 the waves are launched from the mid troposphere, whereas they are launched from the
 258 surface in the UMGA7gws model. In the HadGEM2's scheme (Song & Chun, 2005; Choi
 259 & Chun, 2011), the launched momentum flux is directly related to convective heating
 260 distributed in the vertical between the cloud bottom and cloud top, the launch altitude
 261 being at the cloud top. In this case the launching level can vary between 2km and 15km
 262 typically and the depth of the heating between 1km and 15km We will take the same
 263 inputs to run the WACCM scheme, using the version in Alexander et al. (2021), and de-
 264 spite that in this paper the WACCM scheme was adapted and partly re-written to use
 265 direct satellite observations of convective heating. Note nevertheless that in WACCM,
 266 the heating depth is a quarter of the cloud depth, and ranges between 1km and 4km typ-
 267 ically. Finally, an important difference is that LMDz span harmonics which intrinsic phase
 268 speeds typically range between $-30\text{m/s} < C_{\text{abs}} < 30\text{m/s}$, whereas in both UMGA7gws
 269 and WACCM the choice is made to have absolute phase speeds in the range $-100\text{m/s} <$
 270 $C_{\text{abs}} < 100\text{m/s}$.

271 2.2 Offline parameterization runs

272 To activate the schemes in offline mode we will use ERA-5 hourly data of precip-
 273 itation and 3-hourly data of winds, surface pressure, temperature, cloud liquid and ice
 274 water content at $1^\circ \times 1^\circ$ horizontal grid to mimic a large scale climate model resolution.
 275 Winds, surface pressure, temperature, and water contents are then linearly interpolated
 276 on 1hr time step to be synchronised with precipitation. In the vertical we use data at
 277 67 model levels, taking one every two ERA5 levels again to mimic large scale models ver-
 278 tical resolution but also to speed up calculations. To estimate convective heating rates
 279 vertical profiles, we follow Fueglistaler et al. (2009) and evaluate diabatic heating using
 280 ERA5 hourly data from short range forecast and as a residual between the parameter-
 281 ized temperature tendency and the radiative heatings (longwave plus shortwave). When
 282 needed, we also evaluate the cloud bottom and top altitudes using the cloud water con-
 283 tent (liquid+ice) given in ERA5.

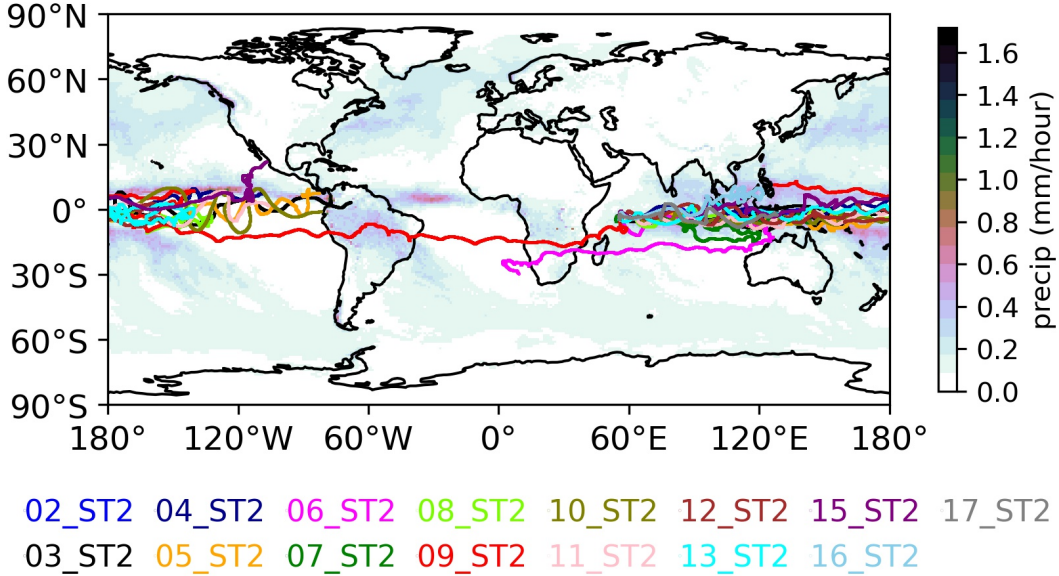


Figure 1. Strateole 2, Phase 2 balloon trajectories taking place between October 2021 and January 2022. Shading presents the precipitation field from ERA5 averaged over the period.

284 **2.3 Strateole 2 balloon observations**

285 The in situ observations we use are from the 8 balloons of the first phase of the Stra-
 286 teole 2 campaign that flew in the lower tropical stratosphere between November 2019
 287 and February 2020 and from the 15 balloons that flew more than one day during the sec-
 288 ond phase of the Strateole 2 campaign, between October 2021 and January 2022. The
 289 trajectories during phase 2 are shown in Figure 1, superimposed upon the averaged pre-
 290 cipitation (the same Figure but for phase 1 is in Lott et al. (2023)). In the MFs calcu-
 291 lated from observations Corcos et al. (2021) distinguish the waves with short periods (1hr-
 292 15mn) from the waves with period up to one day (1d-15mn). They also distinguish the
 293 eastward waves giving positive MF in the zonal direction from the westward waves giv-
 294 ing negative MF. To characterize the QBO condition during the balloon flights, Fig. 2
 295 shows time altitude sections of the equatorial zonal winds and GWD predicted by the
 296 scheme globally and in offline mode using LMDz scheme between 2018-2023. In it we
 297 see that the gravity wave drag is negative (positive) where the zonal mean zonal wind
 298 vertical shear is negative (positive) consistent with the fact that it contributes to the de-
 299 scent of the QBO. We also note that the amplitudes vary between $\pm 0.5\text{m/s/day}$, a range
 300 characteristic of the parameterized GW tendency used in GCMs that produce a quasi-
 301 biennial oscillation (Butchart et al., 2018). The figure also indicates with a green rect-
 302 angle the region and period during which the balloons operated, typically during the end
 303 of easterly QBO phase for both phase 1 and 2. As we shall see this yield quite compa-
 304 rable results during the two phases, and despite the fact that during phase 1 and above
 305 flight altitude the 2nd documented QBO disruption started (Anstey et al., 2021).

306 In the following we will compare the momentum fluxes derived from the balloon
 307 data, emphasize the intrinsic frequencies that the scheme represents (the intrinsic peri-
 308 ods below 1hr) and consider the ERA5 data at the points that are the nearest from
 309 the balloon. The prediction is then made every hour and averaged over the day, partly
 310 because it is the time scale needed for the some schemes to sample realistically a GW
 311 field, and also because it takes around a day for a balloon flight to cover a model grid-

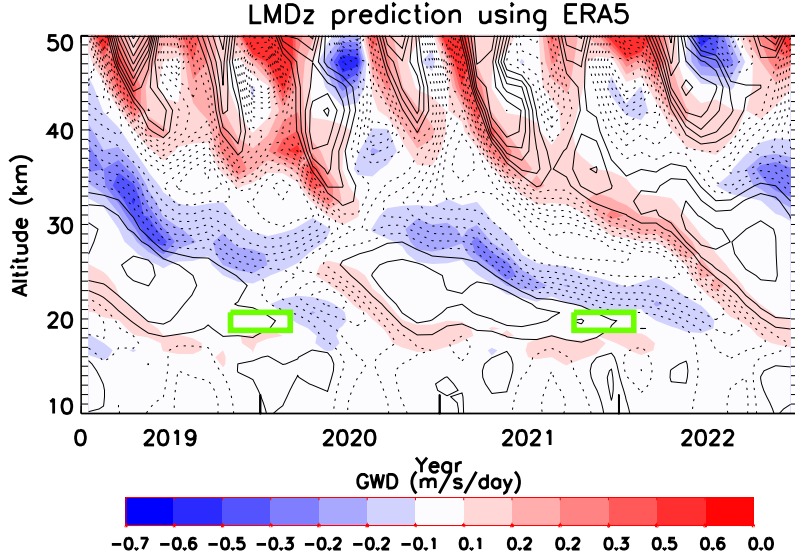


Figure 2. Time vertical sections of the zonal mean zonal wind (CI=10m/s, negative values are dashed and non-orographic gravity wave tendency averaged over the Equatorial band ($-6^{\circ}S - +6^{\circ}N$). Input data are from ERA5 reanalysis and GWs prediction from the LMDz scheme. The 2 green boxes indicate schematically the altitude and time ranges of the Strateole 2 phase 1 and 2 flights considered in this study.

312 scale. Note that some of the sensitivities to these choices are discussed in Lott et al. (2023)’s
 313 conclusion.

314 **3 Results**

315 Figure 3 shows time series of daily values of momentum fluxes predicted by the pa-
 316 rameterizations and measured during balloon flights 2 from strateole 2 phase 1. This is
 317 also the flight shown in Fig. 3 in Lott et al. (2023), and where was also shown the time
 318 series of daily precipitation and zonal wind at flight altitude. The top panel is for the
 319 WMI based schemes, the middle panel for the HDS schemes and the bottom panels for
 320 the schemes relating the GWs fluxes to their sources (3 multiwave, 1 WMI). In all pan-
 321 els the black curves are for the daily observations. For clarity we present results for the
 322 eastward and westward MFs only. Overall ones sees that the schemes predict momen-
 323 tum flux values that somehow compare with the observed one, at least in term of am-
 324 plitude. There are nevertheless significant differences in behaviour. For instance, the IFS’s
 325 schemes present substantial peaks in eastward flux during the second half of the flight,
 326 which is a period during which the zonal wind at flight altitude becomes westward po-
 327 tentially favoring eastward waves, a process we refer to as dynamical filtering in Lott et
 328 al. (2023) (see Figure 3 and Eq. 3 there and the following discussion). Note that in this
 329 paper, was shown that the 3 peaks in measured fluxes around days 60, 75, and 83 also
 330 correspond to dates when there are precipitations near the balloon location. These cor-
 331 respondences made us believe that the relation with convective sources is essential, we
 332 see here that dynamical filtering alone may well be the main cause. Although having smaller
 333 amplitudes, the Figure show that in EC-Earth, the momentum fluxes behave almost as
 334 in IFS. The results from CMAM are quite different nevertheless. In this model it was
 335 chosen to place the launching altitude near the tropopause. As a consequence the daily
 336 series fluctuate less and present long lasting ”plateaus”. Clearly in this model, the dis-
 337 tance between the launching level (100hPa see Table 1) and the balloon altitude is too

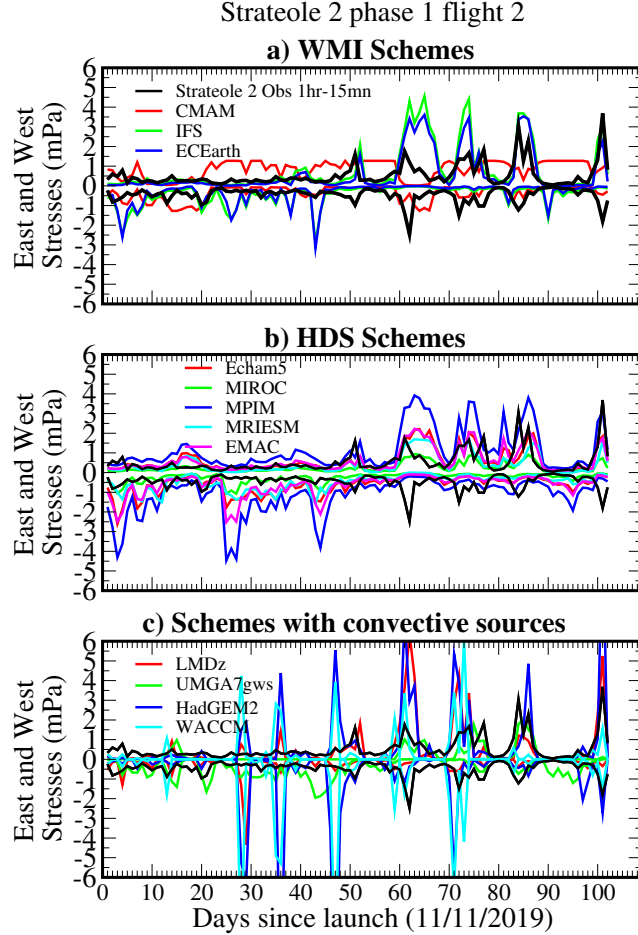


Figure 3. Comparison between daily averaged values of the eastward and westward MFs measured by the balloons during Strateole 2 phase 1 Flight 2 and estimated by the GW schemes at the balloon location and altitude. Colored curves are for the GW schemes predictions using ERA5 and from different models, black curves are for the observed MFs due to the 15mn-1hr GWs. a) WMI schemes; b) HDS Schemes; c) Schemes relating launched MFs with convective sources or precipitations: all multiwaves except UMGA7gws.

338 small for dynamical filtering to be efficient. The second panel for the HDS schemes is
 339 not fundamentally different from what was discussed above. The amplitude and fluctu-
 340 ations are comparable to observed, some schemes predicting values which look either larger
 341 or smaller but staying within the range of observations. The behaviours of the source
 342 related schemes (multiwave for LMDz and HadGEM2, WMI for UMGA7gws) in the last
 343 panel are more contrasted. As expected, there are long periods during which the schemes
 344 predicted small and null momentum fluxes, interrupted by short lasting peaks with
 345 values sometime going beyond $\pm 5\text{mPa}$, values that were never reached by any of the glob-
 346 ally spectral schemes in Panels. 3a) and 3b). In contrast with LMDz and HadGEM2, the
 347 UMGA7gws scheme present smaller amplitude and broader peaks, we attribute this to
 348 that it relates the launched flux to $\sqrt{P_r}$ rather than P_r^2 in LMDz, or the square of heat-
 349 ing in HadGEM2's and WACCM.

350 An other example of timeseries is provided in Fig. 4, which corresponds to a flight
 351 during the second phase of strateole 2. Beyond the fact that the flight is shorter than

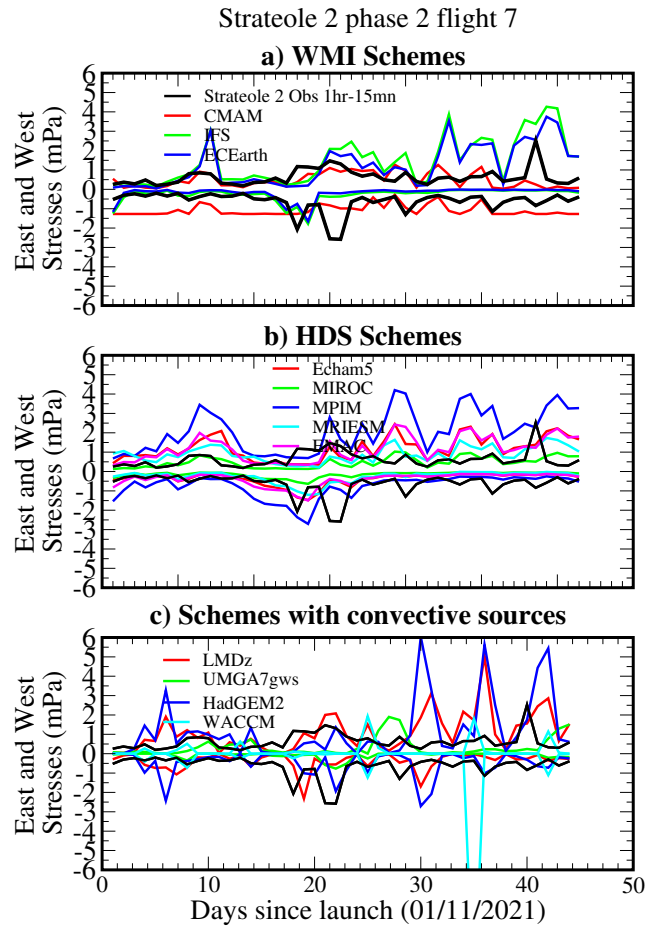


Figure 4. Same as Fig 3 but for Strateole 2 Phase 2 Flight 7.

352 in Fig. 3, a difference in duration that characterizes most of the flights during phase 2
 353 compared to phase 1, the overall behaviours stay about the same, with the spectral schemes
 354 presenting fluctuations with broader peaks, except maybe CMAM, again because the launch-
 355 ing altitude is quite high and dynamical filtering not yet efficient at balloon flight alti-
 356 tude. The last panel also shows that UMGA7gws present long periods with almost no
 357 fluxes, in it, the fact that the launching height is near the surface produces much more
 358 critical level situations during the propagation through the troposphere. Finally, in the
 359 version of WACCM we use, there is extreme outliers at day 33, with values below -10mPa ,
 360 we only found few of them over the entire campaign, and only in WACCM. They trans-
 361 late that WACCM sometimes and rarely predicts extreme values in MFs, but these ex-
 362 treme values significantly contribute to the averaged MFs.

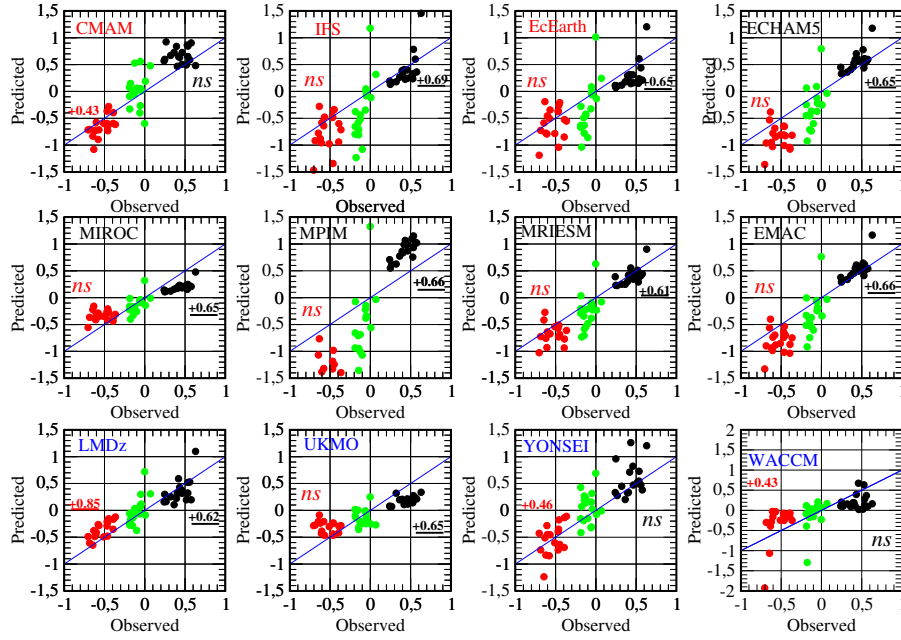


Figure 5. Scatter plot of the momentum fluxes measured by the balloon versus parameterized using different models. Only considered here the 18 balloon flights that last more than a month (East: black; West: red; Cumulated: green). Also shown are the correlations between observations and predictions, 99% significant levels are bold underlined, 95% are bold. Non significant values indicated by "ns". The number of DoF for Pearson test is 23, which is simply the number of balloon flights and which is therefore very conservative, many balloons lasting more than few weeks, whereas the decorrelation time scale of the daily series being well below a week. Color of the names of the WMI, HDS, and convection-related GWs schemes are in red, black and blue respectively. Note the the change of vertical axis in lower left panel.

363 The fact that the different schemes estimate momentum fluxes of about the right
 364 amplitude is summarized in Fig. 5 where the average of the fluxes over the 18 flights that
 365 last more than a month (8 during phase 1, 10 during phase 2) are shown. In this figure
 366 we see that the predicted values align quite well with the observed one, some schemes
 367 having tendency to slightly underestimate the fluxes (MIROC, LMDz), other to over-
 368 estimate them (CMAM, HadGEM2), with the tendency to overestimate being in general
 369 more pronounced for the westward fluxes. The WACCM scheme has a quite distinct
 370 behaviour, most balloons measure quite lower fluxes than measured on average, and few
 371 much larger ones. On average over all flights, we will see that these almost equilibrate

372 but we have to keep in mind that this behaviour is intentional: the WACCM scheme ver-
 373 sion we use have been tuned to produce a very intermittent behaviour and sometime very
 374 strong fluxes Alexander et al. (2021) we cannot exclude that the WACCM model ben-
 375 efits from this. The numbers in each panels also show the correlation between the 18 val-
 376 ues averaged over each flights, showing that the correlations become strong in many mod-
 377 els, at least in the eastward direction. Interestingly some models also have significant medium
 378 to high correlations in the westward direction (CMAM, LMDz, HadGEM2). These tells
 379 that parameterizations can capture well the low frequency variability of the MFs (the changes
 380 with period larger than a month), it is tempting to say that it is good enough for the
 simulation of the QBO.

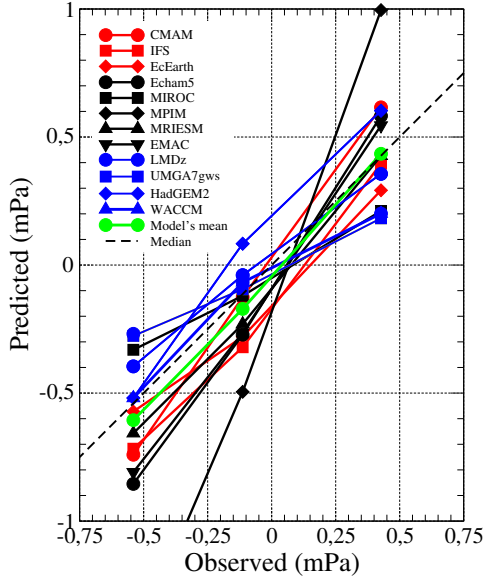


Figure 6. East, West and cumulated zonal momentum fluxes averaged over the Strateole 2 phase 1 and 2 period and according to participating models.

381
 382 The Figure 6 groups the models averaging the eastward and westward fluxes over
 383 all the balloon flights, confirming again that the parameterizations used fall around the
 384 observed values. There is variabilities between the models, but there is no systematic
 385 tendency among the modellers to overstate or understate the MFs flux amplitude. This
 386 is summarized by the green curve which represents the average over models and over bal-
 387 loon flights. The average amplitude of the eastward flux is very near that observed (a
 388 10% overestimation between 0.45mPa in parameterizations against 0.40mPa observed),
 389 whereas the westward flux are overestimated by the models by less than 20% (-0.65mPa
 390 parameterized against -0.55mPa observed). This 10%-20% errors explain the quite large
 391 relative error (50%) in the cumulated flux but for it the large relative error is in good
 392 due to the fact that large positive and negative fluxes opposed each other.

393 The daily series in Figs 3 and 4 also suggest that observations and offline estima-
 394 tions sometimes evolve similarly day after day, a reason could be that both measured
 395 and parameterized MFs are sensitive to dynamical filtering, some schemes also taking
 396 into account sources. In the two examples given here, it is quite apparent in the first (Fig-
 397 ure 3) and for instance for the peaks in the eastward direction as already discussed. Cor-
 398 respondences are less obvious to visualize in the second case (Figure 4) where the evo-
 399 lution of the measured MFs present less variations than the predicted MFs. In Lott et

East	Day Dof	CM AM	IFS	ECE ARTH	Ech am5	MI ROC	MPI M	MRI ESM	EM AC	LMD z	UMG A7gws	HadG EM2	WAC CM
Phase 1	670-216	ns	0.53	0.52	0.43	0.48	0.49	0.44	0.48	0.49	0.34	0.31	ns
Phase 2	621-322	-0.19	0.41	0.38	0.29	0.33	0.34	0.30	0.33	0.40	0.34	0.20	0.26
1+2	1291-538	-0.11	0.49	0.47	0.35	0.41	0.41	0.36	0.40	0.46	0.34	0.26	ns
West	Day Dof	CM AM	IFS	ECE ARTH	Ech am5	MI ROC	MPI M	MRI ESM	EM AC	LMD z	UMG A7gws	HadG EM2	WAC CM
Phase 1	670-216	0.14	ns	ns	ns	ns	ns	ns	ns	0.30	ns	ns	ns
Phase 2	621-322	0.21	0.18	0.16	ns	ns	ns	ns	ns	0.40	ns	0.14	ns
1+2	1291-538	0.17	ns	ns	ns	ns	ns	ns	ns	0.34	0.00	0.11	ns

Table 4. Correlation between observed and measured fluxes, strateole phases 1 and 2. 1% significant values according to 2-sided Pearson test are in bold, 5% are in italic, 'ns' stands for non-significant. To evaluate the number of degree of freedom, we proceed as in Lott et al. (2023) and evaluate for each flight the time lag for which the auto correlations of the daily averaged fluxes fall below 0.1 and divide the number of days by that lag.

al. (2023) these daily variabilities were analysed flights by flights, in some flights the series correlating well whereas in others they do not. The contrast between flights made that in the end the correlations where significant but "medium" in the eastward direction $C \approx 0.5$ and "low" in the westward direction $C \approx 0.3$. Here and in the following, we referred to "medium" positive correlations with $0.3 < C < 0.5$ and small correlations when $0.1 < C < 0.3$. As such a result was obtain from the LMDz parameterization during Strateole 2 phase 1 the coefficients are given again in the 9th column of Table 4. In it are also given the same coefficients but for Phase 2 and measured over the 2 phases. Consistent with the results found for phase 1, we found during phase 2 medium correlation in the Eastward phase ($C = 0.4$) and in the westward phase ($C = 0.40$), the values evaluated over the two phases being medium and small, $C = 0.46$ and $C = 0.34$, respectively. Here and for completeness, note that as in Lott et al. (2023), and to test the significance, we measure the number of Degrees of Freedom (DoF) present in each dataset, and calculate for that the decorrelation time scale, which we take as the lag in day beyond which the lag-autocorrelation of the series falls below 0.2. As this time-lag varies from one series to the other, we give explicitly in column 5, the number of DoF, which is the duration of the flight divided by the decorrelation time scale. Note that for their decorrelation time, we consider for simplicity that evaluated with daily averaged observations, but found that it is not much different from that evaluated with the offline estimates (not shown).

If we now look at the schemes used in the other models, the result are contrasted but quite in agreement. A lot a variations between flights (not shown) the overall behaviour being well summarized in the global correlation coefficients shown in Table 4. First, and as for LMDz, the correlations evaluated using Phase 2 data stay robust when compared to correlations evaluated using phase 1, and whatever is the level of correlation ("medium", "low", or "non significant"). Second, is that many schemes managed to have "medium" correlations ($0.3 < C < 0.5$) in the eastward direction. The schemes having no or small correlations in the eastward direction (CMAM, HadGEM2, and WACCM) are characterized by the fact that in them the launching level is quite high. For instance in CMAM it is always near the tropopause which strongly mitigates dynamical filtering between the launching level and the balloon altitude. Also interesting, the HadGEM2 and WACCM also have low or no correlations, in them and in case of deep convections waves are launched from quite high levels in the troposphere (not shown) suggesting that

433 in them as well and for waves with strong eastward flux, there is not enough space be-
 434 tween launching levels and balloon flight for dynamical filtering to be efficient. The re-
 435 sults in the westward direction are more intriguing, the correlations are always small ex-
 436 cept for 1 scheme (LMDz) and some but "low" correlations are found for two schemes
 437 that launch waves quite near the tropopause (CMAM and HadGEM2). We have diffi-
 438 culties in interpreting this last result, it may be tells that the approaches where some
 439 waves are launched from near the tropopause should not be disregarded, and that launch-
 440 ing from a fixed altitude well in the troposphere fails in some cases. But if this is the case,
 441 the performance of LMDz are somehow in contradiction, in it the launching level is in
 442 the mid troposphere, as many other schemes according to tables 3-2-1. Maybe its skill
 443 come from the fact that LMDz explicitly launch waves according to their intrinsic fre-
 444 quency, a choice that directly affect dynamical filtering, whereas in the globally spectral
 445 schemes the dynamical filtering is more indirect and while in the HadGEM2 and WACCM
 446 scheme the waves are launched according to their absolute frequency. These are more
 447 speculations given here to emphasize the differences that are dynamically significant in
 448 our opinion, what is maybe more interesting to notice that there is room to improve GWs
 449 parameterizations to obtain better fits between predicted and measured fluxes in both
 450 directions of propagation, as illustrates the case of LMDz.

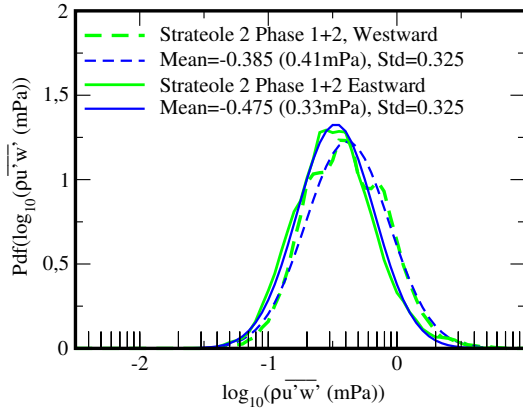


Figure 7. PDFs of daily values of Momentum flux distribution evaluated from Strateole Phases 1 and 2. The PDFs are calculated from histograms of 1291 MFs daily value within intervals of $\Delta(\log_{10} \rho \overline{u'w'}) = 0.05$, thereafter smoothed by a 5 point non-recursive filter with weight (0.1, 0.2, 0.4, 0.2, 0.1). Measured values are in green, log normal fits are in blue. Solid lines are for Eastward, dashed lines are for Westward. Here the log normal probability density function is defined as $P(X) = \frac{1}{\sqrt{2\pi}\sigma} e^{-(X-M)^2/(2S^2)}$, where $X = \log_{10} \rho |u'w'|$, and M and S the mean and standard deviations given in caption.

451 As said in the introduction, more than predicting the right fluxes at the right time,
 452 it is often believed that parameterizations should better be validated against their global
 453 statistical behaviour. A reason is that observed gravity waves show a strong level of in-
 454 termittency such an intermittency impacting the effect of the waves on the large scale
 455 flow and climate in the middle atmosphere. In a recent paper, Green et al. (2023) showed
 456 that this intermittent behaviour is well captured when the GWs MFs have pdfs follow-
 457 ing a log-normal distribution. These authors even concluded that in all directions of prop-
 458 agation, momentum fluxes characteristics could be summarized in terms of the mean and
 459 variance of log normal distributions. As shows Fig. 7, such lognormal distributions also
 460 describe well the Strateole-2 data. In it, one sees that the balloons measure fluxes with
 461 amplitude between 0.1mPa and 10mPa, the pdf of the westward fluxes being shifted to-

ward higher values compared to that for eastward fluxes the shapes being little changed. The Figure also shows that the shifts in pdf between eastward and westward fluxes are also well described by shifts in mean and variance of log-normal distributions.

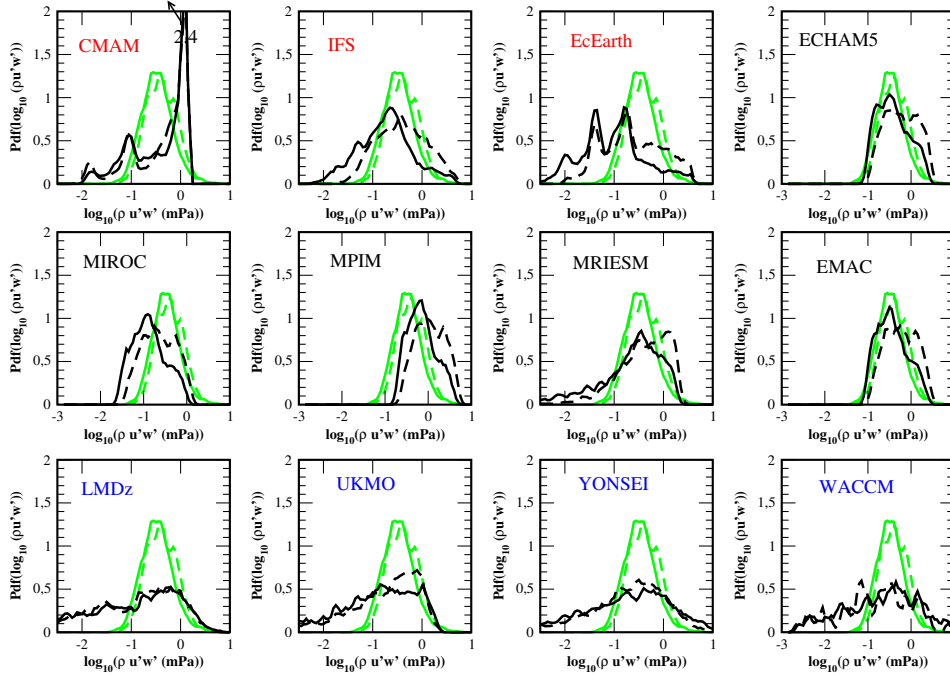


Figure 8. PDFs of daily values of Momentum flux distribution, same method as in Fig. 7. Measured values are in green, estimations using ERA5 data and the parameterizations are in black. Solid lines are for Eastward, dashed lines are for Westward.

Next, and to analyse the QBOi schemes in this framework the Figure 8 presents PDFs of the distributions of the predicted daily values of the momentum fluxes. In it we notice that in the WMI schemes (model names in red) the pdfs are quite broader than the observed pdfs, and often far from log-normal. CMAM and EC-earth for instance present peaks in PDFs not located in the middle of the distribution. Quite remarkably, the HDS schemes (model names in black) seem more realistic: in them the pdfs are narrower and somehow distributed quite along log normal distributions. Importantly, and in all the globally spectral schemes without convective sources (WMI and HDS) the shift of the westward pdf toward higher values compared to the eastward pdf is represented. Finally, the schemes that relate GWs to convection (names in blue) systematically have much broader pdfs, they all present a tail toward small values of the MFs, a tail that is not realistic and that suggest that in them miss a background of wave activity existing even in the absence of convection nearby. In them also, the shift of the westward pdf toward higher values than the eastward pdfs is not much apparent, larger westward fluxes are eventually captured through changes in pdf shape than through translations (see for instance UMGA7gws and HadGEM2). If we now return to the conclusions in Green et al. (2023) that difference in GW momentum fluxes between direction of propagations could essentially be summarized by log-normal pdfs shifted by differences in mean values, one sees that including sources in single column parameterizations is not necessarily skilful to achieve this objective. Finally note that the WACCM scheme has a larger tail toward high values (10mPa) that the other schemes, this tail is consistent with the fact that some balloons have very large fluxes on average (see Fig. 6).

487 **4 Conclusion**

488 The main result of this paper is that state of the art parameterizations of GWs re-
 489 produce reasonably well the momentum flux due to the high-frequency waves (periods
 490 between 15mn and 1hr) deduced from in situ measurements made onboard constant-level
 491 balloons. The parameterizations represent well the eastward and westward values of the
 492 stress and in some cases their variations from day to day. Although the various schemes
 493 performed differently regarding the day to day correlations, our results show that im-
 494 provement can be done in this regard. Some scheme for instance present "medium" cor-
 495 relations in the eastward direction, telling that such correlation level can be reached. In
 496 the westward direction, the day to day correlations are "low", to the best and in 1 model,
 497 we can only say that such a level can be reached in the tropical regions.

498 Due to the low to medium level of correlations we found, we could ask ourselves
 499 if it is mandatory to improve GW schemes according to such a criteria. After all, when
 500 the momentum fluxes are averaged over periods near a month (here we rather consider
 501 averages over balloon flights), the correlations become "medium" to "strong" in the east-
 502 ward direction (see Fig. 5) and sometime medium in the westward direction, which is
 503 probably enough in the context of the QBO forcing, the QBO evolving over time scales
 504 much longer than a month. Also, it is important to recall that the offline testbed we have
 505 used to test the different schemes has been initially designed to evaluate the LMDz scheme
 506 against the strteole 2 data. For this schemes and along the years, we have taken great-
 507 care that the offline setup stay close from the online one. In other words, the offline setup
 508 is not that used in other groups, and is not necessarily optimal for the other parameter-
 509 izations. One should therefore only conclude that that significant daily correlation can
 510 be obtained offline, as illustrates here one scheme in both directian of propagation. One
 511 can also conclude that it is more easy to find significant correlation for eastward waves
 512 than for westward waves, as many schemes show. This is probably related to the phase
 513 of the QBO at the balloons altitudes it would be important to plane an other campaign
 514 in an other phase of the QBO.

515 An other substantial difference concerns the pdfs of the parameterized momentum
 516 fluxes against those of the measured fluxes. The spectral schemes following HDS are those
 517 which behave the more realistically in this respect. The shapes of the pdf present spec-
 518 tra with have one isolated maxima and extend broadly along a log normal curve of about
 519 the right width. They also represent the shift of the pdfs toward larger values for the
 520 westward MFs, something that the WMI schemes also do. These are an interesting re-
 521 sult in itself. In fact, in them the source amplitude is constant, which means that for these
 522 schemes reproducing log normal pdf shifted according to the wave directions only result
 523 from dynamical filtering by the large scale winds: they partly capture the erosion dur-
 524 ing vertical propagation described in (Souprayen et al., 2001). This is important since
 525 log-normal behaviours are significant to the model climate, they capture in good part
 526 the intermittency Green et al. (2023) needed in some models to represent well the final
 527 warmings in the southern hemisphere (de la Cámara et al., 2014) or the fluctuations of
 528 the QBO peridodicity Lott and Guez (2013). Consistent with dynamical filtering, it is
 529 also not surprising that CMAM fails in capturing a log-normal distribution since it launches
 530 waves from quite near the balloon location. The schemes that relate the GWs to con-
 531 vection also present broad spectra, much broader than the spectral schemes, in this sense
 532 they can be viewed as even more intermittent then the spectral schemes, they are also
 533 characterized by long tails toward small values which seem unrealistic. For these schemes
 534 it therefore seems important to introduce a background in wave launching amplitude.
 535 This problem could also be in part corrected out by introducing lateral propagation (Amemiya
 536 & Sato, 2016), a process that is important in the balloon observations used here (Corcos
 537 et al., 2021), but this will not be sufficient over quite large and dry regions.

538 We did not try to fit the parameters of the schemes we use in order to improve daily
 539 correlations or pdfs or both, but we plan to do it in the near future. We have not much

540 data though, but could use the Loon data post-processed in a comparable way as Stra-
541 teale 2 by Green et al. (2023), which would permit to cover much wider regions. We should
542 also test if improving the schemes parameters to improve the fit with observations im-
543 prove or do not degrade the models climate. It may well be that parameterizations com-
544 pensate for potentially resolved equatorial waves for instance, the latter showing a lot
545 of variability between the QBOi models (Holt et al., 2022). Also, we could also hope that
546 a better fit with observed values would help reduced persistent systematic errors in the
547 QBO simulations, one of them being that models underestimate the QBO amplitude in
548 the low stratosphere. Unfortunately, our results so far are not much positive: a common
549 believe is that such an error could well be reduced by launching waves from near the tropopause,
550 the parameterizations which do so here are not much realistic when it comes to predict
551 MFs variabilities (over days or months).

5 Open Research

Balloon data presented in Haase et al. (2018) can be extracted from the STRATEOLE 2 dedicated web site: <https://webstr2.ipsl.polytechnique.fr>

ERA5 reanalysis data are described in Hersbach et al. (2020) and can be extracted from the COPERNICUS access hub: <https://scihub.copernicus.eu/>

The LMDz-6A GCM used for CMIP6 project is described in Hourdin et al. (2020), it can be directly installed from the dedicated webpage: <https://lmdz.lmd.jussieu.fr/utilisateurs/installation-lmdz>

Acknowledgments

This work was supported by the VESRI Schmidt Future project "DataWave".

Appendix: Running the offline code

To run the models parameterizations in offline mode and compare with daily values of momentum fluxes measured during strateole 2, download the file `offline_v9_Strateole_QBOi_Open.tar`, on the web page:

```
wget https://web.lmd.jussieu.fr/~flott/DATA/offline_v9_Strateole_QBOi_Open.tar.gz
```

Then gunzip and do `tar -xvf offline_v9_Strateole_QBOi_Open.tar`

In the directory, `offline_v9_Strateole_QBOi_Open`:

run subdirectory contains the scripts that compile the programs, link to the input dataset and produce various outputs. The Makefile certainly needs to be adapted to the computer.

To launch predictions for Strateole-2 phase 1, launch: `./laun_ph1ball_gwd_era5.sh`
For phase 2, `ph1→ph2`.

prog subdirectory contains all the fortran routines that launch the parameterizations used in 11 QBOi model, except WACCM. Namely:

laun_gwd_era5.f90: Main program loading input data in netcdf format and calculating drag and momentum fluxes at the balloon place.

preci_gwd_LMDz_QBOi.f90: LMDz Multiwaves routines predicting gwdrag from precipitation

gwsat_Modnam.f90: the globally spectral scheme using the Warner and McIntyre (1996)'s scheme version by J. Scinocca.

hinesgw6g_plus_subs.f HDS scheme

gw_ussp_core.f90: The WMI scheme with amplitude keyed to precipitation used in some UMGA7gws runs.

cgwcalc.f90: Multiwave scheme developed for HadGEM2 at YONSEI's university

hourly_ph1(2) contain all the input data for phase 1 and 2 respectively.

STRATEOLE2 hourly values of momentum fluxes are in

`ALL_STRATEOLE2_Balloon_ph1_1day15min.nc`

and

`ALL_STRATEOLE2_Balloon_ph1_1hrs15min.nc`

for the waves with periods between 1day and 15mn and between 1Hr and 15 mn respectively.

ERA5 reanalysis and forecast products, which include winds temperature, cloud liquid and ice water, diabatic heatings, precipitation, surface log pressure, over a $5^{\circ} \times 5^{\circ}$ domain centered at the balloons drifting locations are in

598 Input_ERA5_data_all_variables_balloons_ph1.nc.

599 For phase2, ph1→ph2

600 **output_ph1(2)** contains output subdirectories

601 **Netcdf:** contains the output of the schemes in netcdf format on the vertical col-
 602 umn and over the 5°x5° domain over which the ER5 data are provided. There
 603 is one netcdf dataset by balloons flight each contains output from all the schemes.

604 **Balloon_alt** After post processing by the python scripts launch_script_obs.py,
 605 are extracted the MFs at balloon flight altitude.

606 **python_script**

607 A serie of Python scripts to compare the outputs of the scheme to the balloon data
 608 and produce curves and statistics: correlations, pdfs

609 **launch_script_obs.py:** Reads the balloon flight data of MFs and averaged over
 610 1day and write them in text format (ending with '.dat') and stored in **output/Balloon_alt/obs_output.**

611 **launch_prediction_eachB_ysei.py:** extract from the prediction the values of the
 612 MFs at the balloons place and altitude. Results stored in text format (".dat" in

613 **Balloon_alt/Pred_output_Balloon_altitude/.**

614 The next python scripts are cosmetic in the sense that they use the above two datasets
 615 to make plots of timeseries balloon averaged values, evaluate correlations, and his-
 616 tograms.

617 **timeseries_obs_pred_plot_all.py** Produces a lot of time series for each model
 618 and flights.

619 As a result, you can visualize timeseries of each flight here:

620 **output_ph1/Balloon_alt/figure_timeseries**

621 Histograms here: **output_ph1/histo**

622 Scatter plots and correlations here **output_ph1/correlation**

623 For phase 2, change ph1 in ph2.

624 At these stage, if everything went right wen you have just launched the two ini-
 625 tial scripts, but WACCM is not there.

626 **WACCM** Here are idl routines launching the WACCM code in this language. Launch
 627 idl

628 *IDL* > .r beresflux_offfast.pro

629 *IDL* > BERESFLUX Chose strateole phase, its done when you have done both...

630 **xmgrace** Alternative to calculate the diagnostics, now including WACCM, using for-
 631 tran programs and xmgrace, the programs permit to combine statistics over the
 632 2 phases of Strateole2. Just go in the directory and launch or read the README.sh
 633 file to produce the figures of the paper once the daily timeseries associated with
 634 phase 1 and 2 are produced.

635 **Overleaf** Texmaker file including all the references, figures, and texfiles to compile this
 636 version of the ms.

637

References

638

Achatz, U., Kim, Y.-H., & Voelker, G. S. (2023, 11). Multi-scale dynamics of the interaction between waves and mean flows: From nonlinear WKB theory to gravity-wave parameterizations in weather and climate models. *Journal of Mathematical Physics*, *64*(11), 111101. Retrieved from <https://doi.org/10.1063/5.0165180>

642

Alexander, M. J., Beres, J. H., & Pfister, L. (2000). Tropical stratospheric gravity wave activity and relationships to clouds. *Journal of Geophysical Research: Atmospheres*, *105*(D17), 22299–22309. doi: <https://doi.org/10.1029/2000JD900326>

646

Alexander, M. J., & Dunkerton, T. J. (1999). A Spectral Parameterization of Mean-Flow Forcing due to Breaking Gravity Waves. *J. Atmos. Sci.*, *56*(24), 4167–4182. doi: [10.1175/1520-0469\(1999\)056<4167:ASPOMF>2.0.CO;2](https://doi.org/10.1175/1520-0469(1999)056<4167:ASPOMF>2.0.CO;2)

649

Alexander, M. J., Geller, M., McLandress, C., Polavarapu, S., Preusse, P., Sassi, F., . . . Watanabe, S. (2010). Recent developments in gravity-wave effects in climate models and the global distribution of gravity-wave momentum flux from observations and models. *Q. J. R. Meteorol. Soc.*, *136*, 1103–1124. doi: <https://doi.org/10.1002/qj.637>

654

Alexander, M. J., Liu, C. C., Bacmeister, J., Bramberger, M., Hertzog, A., & Richter, J. H. (2021). Observational validation of parameterized gravity waves from tropical convection in the whole atmosphere community climate model. *Journal of Geophysical Research: Atmospheres*, *126*(7), e2020JD033954. (e2020JD033954 2020JD033954) doi: <https://doi.org/10.1029/2020JD033954>

658

Amemiya, A., & Sato, K. (2016). A new gravity wave parameterization including three-dimensional propagation. *Journal of the Meteorological Society of Japan. Ser. II*, *94*(3), 237–256. doi: [10.2151/jmsj.2016-013](https://doi.org/10.2151/jmsj.2016-013)

662

Andrews, F. G., Holton, J., & Leovy, C. (1987). *Middle atmosphere dynamics*. Academic Press.

664

Anstey, J. A., Banyard, T. P., Butchart, N., Coy, L., Newman, P. A., Osprey, S., & Wright, C. J. (2021). Prospect of increased disruption to the QBO in a changing climate. *Geophysical Research Letters*, *48*(15), e2021GL093058. doi: <https://doi.org/10.1029/2021GL093058>

666

Anstey, J. A., Scinocca, J. F., & Keller, M. (2016). Simulating the qbo in an atmospheric general circulation model: Sensitivity to resolved and parameterized forcing. *Journal of the Atmospheric Sciences*, *73*(4), 1649 - 1665. doi: <https://doi.org/10.1175/JAS-D-15-0099.1>

670

Baldwin, M. P., Gray, L. J., Dunkerton, T. J., Hamilton, K., Haynes, P. H., Randel, W. J., . . . Takahashi, M. (2001). The quasi-biennial oscillation. *Rev. Geophys.*, *39*(2), 179–229. doi: [10.1029/1999RG000007](https://doi.org/10.1029/1999RG000007)

673

Beres, J. H., Garcia, R. R., Boville, B. A., & Sassi, F. (2005). Implementation of a gravity wave source spectrum parameterization dependent on the properties of convection in the whole atmosphere community climate model (waccm). *Journal of Geophysical Research: Atmospheres*, *110*(D10). doi: <https://doi.org/10.1029/2004JD005504>

677

Bushell, A. C., Butchart, N., Derbyshire, S. H., Jackson, D. R., Shutts, G. J., Vosper, S. B., & Webster, S. (2015). Parameterized gravity wave momentum fluxes from sources related to convection and large-scale precipitation processes in a global atmosphere model. *Journal of the Atmospheric Sciences*, *72*(11), 4349–4371. doi: <https://doi.org/10.1175/JAS-D-15-0022.1>

683

Butchart, N., Anstey, J. A., Hamilton, K., Osprey, S., McLandress, C., Bushell, A. C., . . . Yukimoto, S. (2018). Overview of experiment design and comparison of models participating in phase 1 of the sparc quasi-biennial oscillation initiative (“qboi”). *Geoscientific Model Development*, *11*(3), 1009–1032. doi: [10.5194/gmd-11-1009-2018](https://doi.org/10.5194/gmd-11-1009-2018)

686

Charron, M., & Manzini, E. (2002). Gravity waves from fronts: Parameter-

691

- 692 ization and middle atmosphere response in a general circulation model.
693 *Journal of the Atmospheric Sciences*, 59(5), 923 - 941. doi: 10.1175/
694 1520-0469(2002)059<0923:GWFFPA>2.0.CO;2
- 695 Choi, H.-J., & Chun, H.-Y. (2011). Momentum flux spectrum of convective
696 gravity waves. part i: An update of a parameterization using mesoscale
697 simulations. *Journal of the Atmospheric Sciences*, 68(4), 739 - 759. doi:
698 https://doi.org/10.1175/2010JAS3552.1
- 699 Christiansen, B., Yang, S., & Madsen, M. S. (2016). Do strong warm enso events
700 control the phase of the stratospheric qbo? *Geophysical Research Letters*,
701 43(19), 10,489-10,495. doi: https://doi.org/10.1002/2016GL070751
- 702 Corcos, M., Hertzog, A., Plougonven, R., & Podglajen, A. (2021). Observation of
703 gravity waves at the tropical tropopause using superpressure balloons. *Journal*
704 *of Geophysical Research: Atmospheres*, 126(15), e2021JD035165. doi: https://
705 doi.org/10.1029/2021JD035165
- 706 Davini, P., von Hardenberg, J., Corti, S., Christensen, H. M., Juricke, S., Subrama-
707 nian, A., ... Palmer, T. N. (2017). Climate sphinx: evaluating the impact
708 of resolution and stochastic physics parameterisations in the ec-earth global
709 climate model. *Geoscientific Model Development*, 10(3), 1383–1402. Re-
710 trieved from https://gmd.copernicus.org/articles/10/1383/2017/ doi:
711 10.5194/gmd-10-1383-2017
- 712 de la Cámara, A., & Lott, F. (2015). A parameterization of gravity waves emit-
713 ted by fronts and jets. *Geophys. Res. Lett.*, 42(6), 2071-2078. doi: 10.1002/
714 2015GL063298
- 715 de la Cámara, A., Lott, F., & Hertzog, A. (2014). Intermittency in a stochastic
716 parameterization of nonorographic gravity waves. *J. Geophys. Res.: Atmo-*
717 *spheres*, 119(21), 11905-11919. doi: 10.1002/2014JD022002
- 718 de la Cámara, A., Lott, F., Jewtoukoff, V., Plougonven, R., & Hertzog, A. (2016).
719 On the gravity wave forcing during the southern stratospheric final warming
720 in LMDZ. *J. Atmos. Sci.*, 73(8), 3213-3226. doi: https://doi.org/10.1175/
721 JAS-D-15-0377.1
- 722 Eckermann, S. D. (2011). Explicitly Stochastic Parameterization of Nonorographic
723 Gravity Wave Drag. *J. Atmos. Sci.*, 68, 1749–1765. doi: 10.1175/2011JAS3684
724 .1
- 725 Ern, M., Ploeger, F., Preusse, P., Gille, J., Gray, L. J., Kalisch, S., ... Riese, M.
726 (2014). Interaction of gravity waves with the QBO: A satellite perspec-
727 tive. *Journal of Geophysical Research: Atmospheres*, 119, 2329 - 2355. doi:
728 https://doi.org/10.1002/2013JD020731
- 729 Fovell, R., Durran, D., & Holton, J. R. (1992). Numerical simulations of convec-
730 tively generated stratospheric gravity waves. *Journal of Atmospheric Sciences*,
731 49(16), 1427 - 1442. doi: 10.1175/1520-0469(1992)049<1427:NSOCGS>2.0.CO;
732 2
- 733 Fueglistaler, S., Legras, B., Beljaars, A., Morcrette, J.-J., Simmons, A., Tomp-
734 kins, A. M., & Uppala, S. (2009). The diabatic heat budget of the up-
735 per troposphere and lower/mid stratosphere in ecmwf reanalyses. *Quar-*
736 *terly Journal of the Royal Meteorological Society*, 135(638), 21-37. doi:
737 https://doi.org/10.1002/qj.361
- 738 Geller, M. A., Alexander, M. J., Love, P. T., Bacmeister, J., Ern, M., Hertzog, A.,
739 ... Zhou, T. (2013). A comparison between gravity wave momentum fluxes in
740 observations and climate models. *J. Atmos. Sci.*, 26(17).
- 741 Green, B., Sheshadri, A., Alexander, M., Bramberger, M., & Lott, F. (2023). Grav-
742 ity wave momentum fluxes estimated from project loon balloon data. *Journal*
743 *of Geophysical Research: Atmospheres*, Submitted.
- 744 Haase, J. S., Alexander, M. J., Hertzog, A., Kalnajs, L. E., Deshler, T., Davis,
745 S. M., ... Venel, S. (2018). Around the world in 84 days [Dataset]. *Eos*, 99.
746 doi: https://doi.org/10.1029/2018EO091907

- 747 Hersbach, H., Bell, B., Berrisford, P., Hirahara, S., Horányi, A., Muñoz-Sabater,
748 J., ... Thépaut, J.-N. (2020). The ERA5 global reanalysis [Dataset]. *Quar-*
749 *terly Journal of the Royal Meteorological Society*, 146(730), 1999-2049. doi:
750 <https://doi.org/10.1002/qj.3803>
- 751 Hertzog, A. (2007). The stratéole-vorcore long-duration balloon experiment: A per-
752 sonal perspective. *Space Research Today*, 169, 43-48. Retrieved from [https://](https://www.sciencedirect.com/science/article/pii/S1752929807800478)
753 www.sciencedirect.com/science/article/pii/S1752929807800478 doi:
754 [https://doi.org/10.1016/S1752-9298\(07\)80047-8](https://doi.org/10.1016/S1752-9298(07)80047-8)
- 755 Hertzog, A., Alexander, M. J., & Plougonven, R. (2012). On the Intermittency
756 of Gravity Wave Momentum Flux in the Stratosphere. *Journal of the Atmo-*
757 *spheric Sciences*(11), 3433-3448. doi: 10.1175/JAS-D-12-09.1
- 758 Hines, C. O. (1991). The saturation of gravity waves in the middle atmosphere. part
759 ii: Development of doppler-spread theory. *Journal of Atmospheric Sciences*,
760 48(11), 1361 - 1379. doi: [https://doi.org/10.1175/1520-0469\(1991\)048<1361:](https://doi.org/10.1175/1520-0469(1991)048<1361:TSOGWI>2.0.CO;2)
761 [TSOGWI>2.0.CO;2](https://doi.org/10.1175/1520-0469(1991)048<1361:TSOGWI>2.0.CO;2)
- 762 Hines, C. O. (1997). Doppler-spread parameterization of gravity-wave momentum
763 deposition in the middle atmosphere. part 2: Broad and quasi monochromatic
764 spectra, and implementation. *J. Atmos. Solar Terr. Phys.*, 59(4), 387-400. doi:
765 [10.1016/S1364-6826\(96\)00080-6](https://doi.org/10.1016/S1364-6826(96)00080-6)
- 766 Holt, L. A., Lott, F., Garcia, R. R., Kiladis, G. N., Cheng, Y.-M., Anstey, J. A.,
767 ... Yukimoto, S. (2022). An evaluation of tropical waves and wave forcing of
768 the QBO in the QBOi models. *Quarterly Journal of the Royal Meteorological*
769 *Society*, 148(744), 1541-1567. doi: <https://doi.org/10.1002/qj.3827>
- 770 Hourdin, F., Rio, C., Grandpeix, J.-Y., Madeleine, J.-B., Cheruy, F., Rochetin,
771 N., ... Ghattas, J. (2020). LMDZ6A: The atmospheric component of the
772 ipsl climate model with improved and better tuned physics [Software]. *Jour-*
773 *nal of Advances in Modeling Earth Systems*, 12(7), e2019MS001892. doi:
774 <https://doi.org/10.1029/2019MS001892>
- 775 Jewtoukoff, V., Hertzog, A., Plougonven, R., de la Cámara, A., & Lott, F. (2015).
776 Comparison of gravity waves in the southern hemisphere derived from bal-
777 loon observations and the ecmwf analyses. *J. Atmos. Sci.*, 72(9). doi:
778 [DOI:10.1175/JAS-D-14-0324.1](https://doi.org/10.1175/JAS-D-14-0324.1)
- 779 Jewtoukoff, V., Plougonven, R., & Hertzog, A. (2013). Gravity waves generated by
780 deep tropical convection: Estimates from balloon observations and mesoscale
781 simulations. *Journal of Geophysical Research: Atmospheres*, 118(17), 9690-
782 9707. doi: <https://doi.org/10.1002/jgrd.50781>
- 783 Jöckel, P., Kerkweg, A., Pozzer, A., Sander, R., Tost, H., Riede, H., ... Kern,
784 B. (2010). Development cycle 2 of the modular earth submodel sys-
785 tem (messy2). *Geoscientific Model Development*, 3(2), 717-752. doi:
786 [10.5194/gmd-3-717-2010](https://doi.org/10.5194/gmd-3-717-2010)
- 787 Kang, M.-J., Chun, H.-Y., & Kim, Y.-H. (2017). Momentum flux of convective
788 gravity waves derived from an offline gravity wave parameterization. part i:
789 Spatiotemporal variations at source level. *Journal of the Atmospheric Sci-*
790 *ences*, 74(10), 3167 - 3189. doi: 10.1175/JAS-D-17-0053.1
- 791 Lane, T. P., & Moncrieff, M. W. (2008). Stratospheric gravity waves generated by
792 multiscale tropical convection. *J. Atmos. Sci.*, 65, 2598-2614. doi: DOI:10
793 [.1175/2007JAS2601.1](https://doi.org/10.1175/2007JAS2601.1)
- 794 Lindzen, R. S. (1981). Turbulence and stress owing to gravity wave and tidal break-
795 down. *J. Geophys. Res.*, 86(C10), 9707-9714. doi: 10.1029/JC086iC10p09707
- 796 Liu, C., Alexander, J., Richter, J., & Bacmeister, J. (2022). Using trmm latent
797 heat as a source to estimate convection induced gravity wave momentum
798 flux in the lower stratosphere. *Journal of Geophysical Research: Atmo-*
799 *spheres*, 127(1), e2021JD035785. (e2021JD035785 2021JD035785) doi:
800 <https://doi.org/10.1029/2021JD035785>
- 801 Lott, F., & Guez, L. (2013). A stochastic parameterization of the gravity waves due

- 802 to convection and its impact on the equatorial stratosphere. *J. Geophys. Res.*,
 803 *118*(16), 8897-8909. doi: 10.1002/jgrd.50705
- 804 Lott, F., Guez, L., & Maury, P. (2012). A stochastic parameterization of non-
 805 orographic gravity waves: Formalism and impact on the equatorial strato-
 806 sphere. *Geophys. Res. Lett.*, *39*(6), L06807. doi: 10.1029/2012GL051001
- 807 Lott, F., Rani, R., Podglajen, A., Codron, F., Guez, L., Hertzog, A., & Plougonven,
 808 R. (2023). Direct comparison between a non-orographic gravity wave drag
 809 scheme and constant level balloons. *Journal of Geophysical Research: Atmo-*
 810 *spheres*, *128*(4), e2022JD037585. doi: <https://doi.org/10.1029/2022JD037585>
- 811 Manzini, E., McFarlane, N. A., & McLandress, C. (1997). Impact of the doppler
 812 spread parameterization on the simulation of the middle atmosphere circula-
 813 tion using the ma/echam4 general circulation model. *Journal of Geophysical*
 814 *Research: Atmospheres*, *102*(D22), 25751-25762. doi: 10.1029/97JD01096
- 815 Naoe, H., & Yoshida, K. (2019). Influence of quasi-biennial oscillation on the bo-
 816 real winter extratropical stratosphere in qboi experiments. *Quarterly Journal*
 817 *of the Royal Meteorological Society*, *145*(723), 2755-2771. doi: [https://doi.org/](https://doi.org/10.1002/qj.3591)
 818 [10.1002/qj.3591](https://doi.org/10.1002/qj.3591)
- 819 Orr, A., Bechtold, P., Scinocca, J., Ern, M., & Janiskova, M. (2010). Improved mid-
 820 dle atmosphere climate and forecasts in the ecmwf model through a nonoro-
 821 graphic gravity wave drag parameterization. *Journal of Climate*, *23*(22), 5905
 822 - 5926. doi: <https://doi.org/10.1175/2010JCLI3490.1>
- 823 Piani, C., Norton, W. A., & Stainforth, D. A. (2004). Equatorial stratospheric
 824 response to variations in deterministic and stochastic gravity wave parame-
 825 terizations. *Journal of Geophysical Research: Atmospheres*, *109*(D14). doi:
 826 <https://doi.org/10.1029/2004JD004656>
- 827 Plougonven, R., Jewtoukoff, V., de la Cámara, A., Lott, F., & Hertzog, A. (2017).
 828 On the relation between gravity waves and wind speed in the lower strato-
 829 sphere over the southern ocean. *J. Atmos. Sci.*, *74*(4), 1075-1093. doi:
 830 [10.1175/JAS-D-16-0096.1](https://doi.org/10.1175/JAS-D-16-0096.1)
- 831 Pohlmann, H., Müller, W. A., Kulkarni, K., Kameswarrao, M., Matei, D., Vamborg,
 832 F. S. E., ... Marotzke, J. (2013). Improved forecast skill in the tropics in the
 833 new miklip decadal climate predictions. *Geophysical Research Letters*, *40*(21),
 834 5798-5802. doi: <https://doi.org/10.1002/2013GL058051>
- 835 Rabier, F., Boucharde, A., Brun, E., Doerenbecher, A., Guedj, S., Guidard, V.,
 836 ... Steinle, P. (2010, January). The Concordiasi Project in Antarctica.
 837 *Bulletin of the American Meteorological Society*, *91*(1), 69-86. Retrieved
 838 from <https://hal-insu.archives-ouvertes.fr/insu-00562459> doi:
 839 [10.1175/2009BAMS2764.1](https://doi.org/10.1175/2009BAMS2764.1)
- 840 Richter, J. H., Sassi, F., & Garcia, R. R. (2010a). Toward a physically based gravity
 841 wave source parameterization in a general circulation model. *Journal of the At-*
 842 *mospheric Sciences*, *67*(1), 136 - 156. doi: 10.1175/2009JAS3112.1
- 843 Richter, J. H., Sassi, F., & Garcia, R. R. (2010b). Toward a Physically Based Grav-
 844 ity Wave Source Parameterization in a General Circulation Model. *J. Atmos.*
 845 *Sci.*, *67*(1), 136-156. doi: 10.1175/2009JAS3112.1
- 846 Roeckner, E., Brokopf, R., Esch, M., Giorgetta, M., Hagemann, S., Kornblueh, L.,
 847 ... Schulzweida, U. (2006). Sensitivity of simulated climate to horizontal
 848 and vertical resolution in the echam5 atmosphere model. *Journal of Climate*,
 849 *19*(16), 3771 - 3791. doi: <https://doi.org/10.1175/JCLI3824.1>
- 850 Scaife, A. A., Butchart, N., Warner, C. D., & Swinbank, R. (2002). Impact of a
 851 spectral gravity wave parameterization on the stratosphere in the met office
 852 unified model. *Journal of the Atmospheric Sciences*, *59*(9), 1473 - 1489. doi:
 853 [https://doi.org/10.1175/1520-0469\(2002\)059<1473:IOASGW>2.0.CO;2](https://doi.org/10.1175/1520-0469(2002)059<1473:IOASGW>2.0.CO;2)
- 854 Scinocca, J. F. (2003). An accurate spectral nonorographic gravity wave drag pa-
 855 rameterization for general circulation models. *Journal of the Atmospheric Sci-*
 856 *ences*, *60*(4), 667 - 682. doi: [https://doi.org/10.1175/1520-0469\(2003\)060<0667:](https://doi.org/10.1175/1520-0469(2003)060<0667:)

- 857 AASNGW)2.0.CO;2
- 858 Serva, F., Cagnazzo, C., Riccio, A., & Manzini, E. (2018). Impact of a stochastic
859 nonorographic gravity wave parameterization on the stratospheric dynamics of
860 a general circulation model. *Journal of Advances in Modeling Earth Systems*,
861 *10*(9), 2147–2162. doi: <https://doi.org/10.1029/2018MS001297>
- 862 Song, I.-S., & Chun, H.-Y. (2005). Momentum flux spectrum of convectively
863 forced internal gravity waves and its application to gravity wave drag pa-
864 rameterization. part i: Theory. *J. Atmos. Sci.*, *62*(1), 107–124. doi:
865 <https://doi.org/10.1175/JAS-3363.1>
- 866 Souprayen, C., Vanneste, J., Hertzog, A., & Hauchecorne, A. (2001). Atmospheric
867 gravity-wave spectra: A stochastic approach. *J. Geophys. Res.*, *106*, 24,071-
868 24,086.
- 869 Warner, C. D., & McIntyre, M. E. (1996). On the propagation and dissipation
870 of gravity wave spectra through a realistic middle atmosphere. *J. Atmos. Sci.*,
871 *53*(22), 3213–3235. doi: 10.1175/1520-0469(1996)053<3213:OTPADO>2.0.CO;
872 2
- 873 Warner, C. D., & McIntyre, M. E. (1999). Toward an ultra-simple spectral grav-
874 ity wave parameterization for general circulation models. *Earth, Planets and*
875 *Space*, *51*, 475–484. doi: 10.1186/BF03353209
- 876 Watanabe, S., Hajima, T., Sudo, K., Nagashima, T., Takemura, T., Okajima, H., ...
877 Kawamiya, M. (2011). Miroc-esm 2010: model description and basic results of
878 cmip5-20c3m experiments. *Geoscientific Model Development*, *4*(4), 845–872.
879 doi: 10.5194/gmd-4-845-2011